



Perspective

The Importance of Interphases in Energy Storage Devices: Methods and Strategies to Investigate and Control Interfacial Processes

Chiara Ferrara , Riccardo Ruffo and Piercarlo Mustarelli * 

Department of Materials Science, University of Milano-Bicocca, and GISEL-INSTM, Via Cozzi 55, 20125 Milano, Italy; chiara.ferrara@unimib.it (C.F.); riccardo.ruffo@unimib.it (R.R.)

* Correspondence: piercarlo.mustarelli@unimib.it

Abstract: Extended interphases are playing an increasingly important role in electrochemical energy storage devices and, in particular, in lithium-ion and lithium metal batteries. With this in mind we initially address the differences between the concepts of interface and interphase. After that, we discuss in detail the mechanisms of solid electrolyte interphase (SEI) formation in Li-ion batteries. Then, we analyze the methods for interphase characterization, with emphasis put on in-situ and operando approaches. Finally, we look at the near future by addressing the issues underlying the lithium metal/electrolyte interface, and the emerging role played by the cathode electrolyte interphase when high voltage materials are employed.

Keywords: interphase; batteries; characterization



Citation: Ferrara, C.; Ruffo, R.; Mustarelli, P. The Importance of Interphases in Energy Storage Devices: Methods and Strategies to Investigate and Control Interfacial Processes. *Physchem* **2021**, *1*, 26–44. <https://doi.org/10.3390/physchem1010003>

Academic Editor: Jacinto Sá

Received: 11 March 2021

Accepted: 6 April 2021

Published: 13 April 2021

Publisher's Note: MDPI stays neutral with regard to jurisdictional claims in published maps and institutional affiliations.



Copyright: © 2021 by the authors. Licensee MDPI, Basel, Switzerland. This article is an open access article distributed under the terms and conditions of the Creative Commons Attribution (CC BY) license (<https://creativecommons.org/licenses/by/4.0/>).

1. Introduction

There is a growing discussion about the meaning and the role of interface/interphase in functional materials and devices [1]. Indeed, an interface is a two-dimensional boundary between phases in thermodynamic equilibrium. On the other hand, this could be seen just as a theoretical statement, as dynamic equilibrium will take place at the atomic scale. As an example, non-zero equilibrium exchange currents exist when electrodes are placed in ionic solutions [2]. Therefore, in the nanometer and sub-nanometer range, the concept of interface must be replaced by (or considered together with) that of interphase, a three-dimensional layer which in the solid state can be characterized by a different crystalline structure, microstructure, physico-chemical and functional properties with respect to the parent phases in contact [3]. Obviously, the role of the interphase becomes more and more important as particle/phase dimensions decrease.

Extended interphases are of relevance in electrochemical devices such as batteries, fuel cells, sensors and supercapacitors. Concerning lithium-ion batteries (LIBs), which at present are the market choice for both automotive and grid storage [4], a fundamental role to date has been played by the solid electrolyte interphase (SEI) between the anode (graphite) and the liquid electrolyte [5,6]. SEI is a passivation layer in the range ~0.01–0.1 μm, due to electrolyte degradation products which are formed at low electric potential during the first cycles of the battery. Mechanical and chemical SEI stability is of paramount importance for the life cycle of state-of-the-art LIBs (generation 3a) which operate below 4.3 V vs. Li⁺/Li [6]. Next generation batteries (generations 3b and 4) will work at higher potential (up to 4.8 V), which will cause a major role of the cathode/electrolyte interphase (CEI), formed by the high voltage decomposition of both cathode and electrolyte [7,8]. This will require a careful tailoring of the electrolyte/cathode interface. The higher the voltage, the more important the interfacial control.

In this perspective we will address the role of the interphases in lithium batteries. We will put emphasis on the mechanisms and reactions at the basis of SEI formation (Section 2).

Then, we will focus on advanced (in-situ, operando) investigation methods for interphase characterization and monitoring (Section 3). Finally, we will give a look into the next future by considering some relevant issues including Li-metal dendrites control, dynamic SEI formation, CEI control and the role of carbon (Section 4).

2. Mechanisms of SEI Formation

The Graphite/SEI Intephase

The history of the development of graphite in LIBs is the most significant example of the importance of controlling interfaces in energy storage [9]. The possibility of intercalating lithium ions in graphite to form the LiC_6 structure was known since 1975, thanks to experiments carried out in molten lithium and compressed graphite [10]. However, earlier experiments in presence of liquid electrolytes failed due to the delamination of graphite in the presence of carbonate solvents, in particular propylene carbonate (PC), at that time the most favorable solvent in terms of a compromise between dielectric properties and viscosity [11]. The electrochemical reversible intercalation of lithium in graphite at room temperature was successfully demonstrated firstly in polymer electrolytes (poly(ethylene oxide), PEO) [12], and later in mixtures of liquid carbonates including ethylene carbonate (EC) [13]. Similar investigations were also carried out at the same time in Japan [14], which led to the first LIB in 1991 [15], and to the wide use of graphite since 1993 [16]. The role of EC in enabling the reversibility of the intercalation reaction was understood in the framework of the solid electrolyte interface (SEI) model developed a few years earlier by Peled [5] to explain the unusual stability of some solvents in extremely reducing conditions, i.e., in contact with alkali metals. Thus, the formation during the first lithiation (first cathodic reaction) of a stable and compact SEI is the key to understand the working mechanism of graphite at potential lower than 0.8 V vs. Li^+/Li (Figure 1). This SEI was widely investigated, and its nature is described in a number of reviews [17,18].

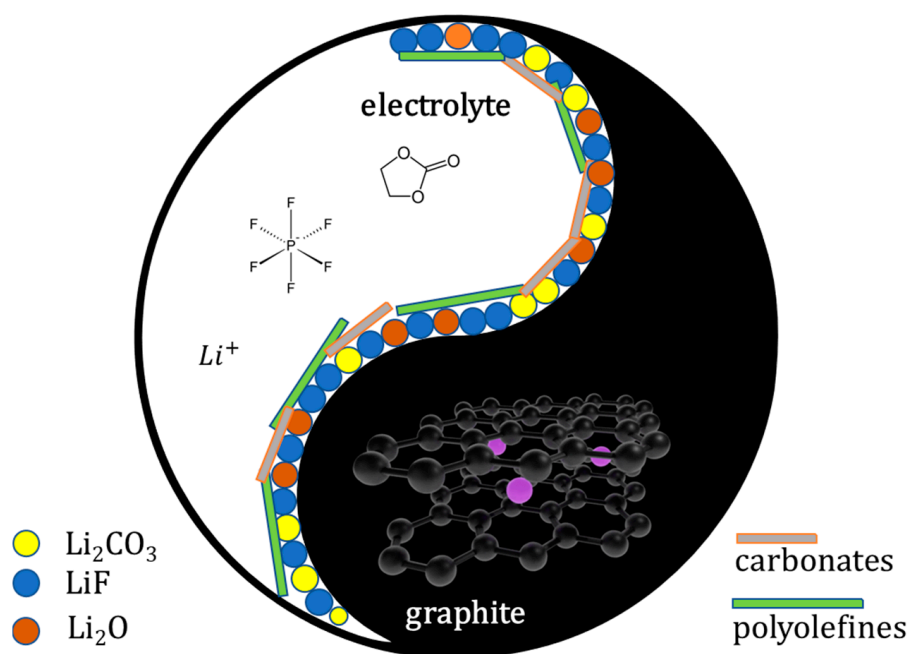


Figure 1. Schematic representation of the SEI at the electrolyte/graphite interface highlighting the inorganic and organic chemical nature of the layer.

At the graphite interface, the interphase is made up of a dense layer of nanometric grains of inorganic salts (Li_2CO_3 , LiF , Li_2O) formed by the decomposition reaction of the electrolyte. This dense layer prevents the contact between the active material and the electrolyte itself, arresting its further decomposition but allowing, at the same time, Li ions to pass through. Between the dense inorganic layer and the solution bulk there is a

secondary layer made by organic compounds such as poly(olefins) and carbonates, which are also produced by the decomposition of the solvent. The role of this external layer, having much higher ionic conductivity, is fundamental because it favors the formation of the dense inner layer, preventing the penetration of small molecules into the graphite structure which could lead to delamination. This can explain the contradictory behavior between EC and PC, two very similar molecules that differ just for the presence of a methyl group attached to the ring. In fact, upon reduction, EC generates three dimensional branched polymeric chains which passivate the internal shell, while PC forms ternary radicals which can give substituted olefins or linear polymeric chains unable to form a dense protecting layer [19,20].

The nature and the thickness of the SEI layer depends on two main factors: the surface morphology and the electrolyte composition. Battery-grade graphite for LIBs has usually spherical morphology with micrometric particle sizes. This guarantees the presence of an extended edge plane surface responsible for the lithium-ion intercalation, which does not take place through the denser basal planes [9]. The anisotropic nature of the graphite structure has also an effect on the nature of the SEI layers. The “real” SEI is indeed observed only at the edge plane interface, with a thickness of about 35 nm and the already described chemical composition [21]. In contrast, the basal SEI is thinner (7 nm), it is made mainly by organic decomposition products, it continues to grow during cycling, and it has the only role of surface passivation without ion transport properties [22,23].

Since 1990, the improvement of the performance of graphite anodes was obtained thanks to the more careful control of the SEI, obtained by working on both passivation and ion transport properties [24]. Thus, additives such as vinylene carbonate (VC) [25] and fluoroethylene carbonate (FEC) [26] were developed to improve the graphite first cycle Coulomb efficiency, the rate capability and the capacity retention.

3. Interphase Investigation Methods

LIBs active components and materials were successfully characterized with traditional ex-situ approaches (e.g., X-rays diffraction, electrochemical impedance spectroscopy (EIS)), which are easy to implement, generally inexpensive, and accessible in many laboratories. Ex-situ characterization of pure pristine components (e.g., cathode and anode powders or electrodes deposited on the current collectors) led to reliable information on both the structure and functional properties of such materials, allowing researchers to infer their behavior when embodied in the final device and under working conditions.

On the contrary, ex-situ investigation of LIB interfaces/interphases can be challenging, as this involves the disassembly of the cell to expose the layer of interest. This operation can lead to modification of the peculiar microstructure and texture of the surface itself and can also alter the composition of these layers, mainly due to H₂O/O₂ exposure even at very low concentrations. For these reasons, the in-situ (full device, not working) and operando (full device under working conditions) approaches, even if more expensive, less accessible, and more challenging are better tools for the investigation of the formation, structure, and evolution of LIBs interphases.

The major limitation for the implementation of in-situ and *operando* methods is the need of dedicated experimental set-up, dedicated cell design, and cell assembly. A second relevant point to be considered for the investigation of the interphases is their intrinsic nature of 3D layers with variable thickness, complex microstructure and composition. Thus, when considering the investigation technique of choice, spatial resolution must be considered in addition to sensitivity and selectivity.

Moreover, as the interphase is a layer evolving under working conditions, also time resolution is a relevant parameter for dynamic characterization of the SEI and CEI. Indeed, both SEI and CEI may undergo significant evolution during the working cycles of the battery in terms of volumetric expansion/contraction, phase transitions, parasitic reactions and both reversible and irreversible phases formation. Finally, a thorough evaluation may require spanning over several orders of magnitude both in spatial and time domains, and

thus inevitably resorts to the use of multi-techniques approach offering complementary information. In the following, the most relevant techniques are discussed with some examples of application in the study of LIBs interphases. Table 1 reports the main advantages and disadvantages of the different techniques with respect to their capability of investigating interfaces/interphases.

3.1. Diffraction-Based Techniques

Diffraction techniques are among the most exploited methods to characterize battery materials, and chiefly the electrodes [27–31]. The main advantages offered by diffraction methods are: (i) the versatility related to use different radiation sources (Xrays, neutron, electrons, offering complementary information, penetration depth, and sensitivity), (ii) the non-destructive nature of the measurement, and (iii) the possibility to detect both crystalline and amorphous components. However, some major complications must be considered when the in-situ and operando approaches are considered. Indeed, dedicated cells with specific design are needed to minimize the undesired radiation interaction with battery components such as case, current collectors and separators [27]. Moreover, special radiation sources (e.g., synchrotron [30]) are required to allow for fast acquisitions. Finally, this is a bulk technique which does not allow spatial resolution, but for tomography and microtomography applications (see Section 3.4) [30]. Finally, depending on the selected radiation source (laboratory X-rays, synchrotron light, neutrons, electrons) the data acquisition time can vary significantly, highly impacting on the possible time resolution.

The structural and compositional evolution of the electrode was reported by several publications [27–37]. The investigation of SEI formation with diffraction techniques is still challenging and only few examples were reported based on XRD [32–34] and neutron diffraction [35–37]. The use of in-situ fast XRD measurements allowed for the detection of the formation of LiF crystallites on the graphene surface and for revealing their texture [32]; the compositional analysis of the SEI layer was further confirmed by XPS analysis. XRD allowed also for the monitoring of the degradation of the cathode material and the SEI formation mechanism [34]. Neutron diffraction experiments were exploited for the analysis of commercial 18,650-type cell and the structural evolution of the electrodes and the SEI layer were reported [37].

With respect to X-rays, neutron diffraction offers higher sensitivity to detect lithium and other light elements, and thus can be preferred for the investigation of SEI layers. At the same time, neutron diffraction measurements require big facilities and longer acquisition times due to the lower intensity of the incident radiation beams. The information that can be obtained on the interphases is related to the identification of the constituent phases and their crystal/amorphous structures. Many of the components in the SEI and CEI layers are organic, amorphous, or small inorganic crystals, thus the analysis of the total diffuse radiation, and in particular the use of pair distribution function (PDF) can be also exploited to better characterize these species [38,39].

3.2. X-rays/Electron Absorption Spectroscopies

Beside diffraction, X-rays are a versatile probe due to the wide range of interactions with matter, including absorption and reflection. X-rays absorption spectroscopy (XAS), is indeed a powerful tool for the investigation of the atomic structure of the LIBs materials and constituents, leading to the identification of local coordination and oxidation numbers of the different atomic species. It offers good sensitivity and selectivity, can be used for the characterization of crystalline and amorphous components, and the acquisitions are generally fast enough to allow for operando studies under cycling on the time scale of the electrochemical processes [28,40–43]. As for XRD, high-intensity sources are preferred for in-situ analysis, thus synchrotron light can be required together with dedicated cell assembly including special precautions (e.g., free-standing electrodes, inert atmosphere, use of specific electrodes [44,45]). As for the diffraction studies, also in this case the

investigation of the interphases is still challenging but some pioneering works have been reported [43–47].

Similar to XAS, X-rays photoelectron spectroscopy (XPS), was widely exploited for the ex-situ characterization of electrode surfaces. In-situ XPS is now receiving particular attention for the characterization of interfaces due to the ability: (i) to detect almost all the elements with very low detection limits, and (ii) to perform a surface-sensitive analysis. Both laboratory and synchrotron radiation can be exploited for such analyses [48]. One of the major limitations is the requirement of ultrahigh vacuum, which is not compatible with the commonly used liquid electrolytes and with the non-conductive nature of the SEI layer. While ex-situ SEI characterization has been widely exploited and reviewed [48,49], in-situ investigations are still facing the challenges of cell design and proper experimental setup [50–53]. However, it is exploited to monitor the composition of the species formed during the electrochemical reaction at the electrode surface with no spatial resolution. A significant example of the combined application of XRD, XAS, and XPS measurements was reported by Deng et al. who were able to follow the cathode surface degradation mechanism and products in an all-solid state LIBs system [43]. In particular, XPS analysis was exploited for the identification of the chemical species and compounds constituting the CEI layer, formed upon oxidation of the cathode reacting with the solid electrolyte, demonstrating the ability of this technique to address such issues.

3.3. Reflectometry and Scattering

Apart from the chemical composition and structure of the constituents, also morphological features of the interphase such as roughness, density, and thickness, do play a crucial role in determining its behavior in the working device. Reflectometry is one of the best tools to address these aspects. It is generally used for the analysis of surfaces and thin films and can exploit, similarly to diffraction, different radiation sources (X-rays, neutrons). X-rays reflectometry (XRR) can monitor the surface in terms of structural information, density, thickness, roughness of a layer. This can be done during in-situ evolution of the layer and down to the atomic scale, thus XRR is really promising for the investigation of the electrodes/electrolyte interface/interphase. Again, up to now only few examples were reported in literature due to the complexity of the cell scheme and design [54,55]. Neutron reflectometry is similar to XRR as far as the working principles are considered, but offers higher penetration depth and higher resolution, thus it is particularly appealing for the SEI investigation under operando conditions [56–58]. Neutron reflectometry was exploited for the operando investigation of irreversible capacity losses correlated with SEI formation in a Si-based LIB [56]. Indeed, neutron reflectometry offers the possibility to obtain quantitative information on the Li concentration in the amorphous SEI layer. Neutrons are also exploited for the small angle neutron scattering (SANS) and inelastic neutron scattering (INS) techniques, providing information about the size, shape, volume of nanostructures of the interphase layers in the range of 5–200 nm [59–64].

3.4. Imaging and Microscopy

The morphology of the interfaces can be monitored by exploiting imaging techniques based on different radiation sources. X-rays imaging can be declined on several techniques, including tomography (XRT), and transmission microscopy (XTM), which offer spatial resolution up to ~20 nm using synchrotron radiation, and can be used to collect 2D images, as well all to reconstruct 3D images, thus offering a unique insight into the visualization of interfaces/interphases [36,65–71]. Neutron radiation can also be exploited for acquisition of 2D and 3D images, so allowing to monitor Li dynamics and distribution, gas evolution and SEI formation [72–76]. Neutron depth profiling (NDP) was used for the selective detection of ^6Li isotopes to monitor the lithium mass transport within the cell under working conditions [77–79]. This allows for the detection of both reversible and irreversible formation of interfacial layers and their evolution. At the same time, this analysis is more challenging due to: (i) low neutron flux (thus not allowing for fast time resolution),

(ii) issues related to magnetic interactions and detection of magnetic structures, and (iii) strong background from hydrogenated species, such as polymer of the binder and separator and electrolyte components.

More traditional and less demanding microscopy techniques were also exploited for the investigation of interfaces/interphases. Traditional optical microscopy, OM, offers relatively low spatial resolution (~200 nm). Therefore, only microstructural features can be observed, whereas the formation and evolution of the nanometric SEI components is challenging. Generally, OM is used for the direct observation of dendrites and the follow up of the electrode evolution in terms of volume and stress cycling [80,81]. Higher spatial resolution (~10 nm) can be obtained with scanning electron microscopy, SEM. At the same time, high vacuum and electrically conductive samples are generally needed, which limit the possible applications for in-situ studies to electrodes and solid and semi-solid electrolytes. Dedicated cells and configurations were developed trying to overcome the major limitations [82,83] and pioneering works for the study of interface/interphase were already reported [82,84,85]. Transmission electron microscopy, TEM, suffers of similar and even greater problems related to sample preparation and cell configuration. Therefore, only a few setups have been developed to date [86–88]. Resolution at the atomic level and fast acquisition allow to follow the dynamics of the systems under study. Images and movies can be obtained, and impressive results were recently reported combining information coming from imaging and diffraction analysis [89–95]. Recently, other innovative techniques such as scanning electrochemical microscopy, SECM, and cryogenic electron microscopy, CEM, were proposed for in-situ SEI investigation [96,97]. The variety of experimental setups, possible techniques, and variety of information that can be obtained were reviewed, highlighting the versatility of TEM analysis [93]. In particular, TEM was widely exploited to detect the lithiation of the electrode materials, to observe the volumetric expansion of the electrodes, to detect the growth of passivation layers/particles as it enables for direct visualization of these phenomena with nanometric resolution and, combining diffraction information, for the detection of the crystal phases.

Atomic force microscopy, AFM, was exploited as alternative to SEM and OM thanks to the higher resolution (sub-nanometer range), the possibility to obtain 3D images, and less limitations on the nature of the samples (no needs for conductive samples and full compatibility with liquids). AFM generates a tomographic image of the surface of the investigated sample. For these reasons it is particularly suitable for the study of SEI formation and evolution, particularly for the evaluation of the thickness and stability with time [98–101].

3.5. Other Spectroscopies and Electrochemistry-Based Approaches

The chemical composition and identification of the species constituting the SEI and CEI layers may be investigated via the traditional spectroscopic techniques such as FTIR, Raman or electron energy loss spectroscopy (EELS) [102]. FTIR allows for implementation of several modes (transmission, reflectance, reflection absorption, attenuated total reflection) for both ex-situ and in-situ investigations [103,104], and it is generally preferred to Raman due to strongest signals and fastest acquisition. Moreover, FTIR is highly sensitive to organic components, thus it can be exploited for the follow up of processes such as electrolyte decompositions, gas evolution, solvent intercalation, SEI formation, identification of the role of additives, changes in concentration of different species, coordination of different species near the electrode surface. Similar to FTIR, Raman was exploited using different cells schemes [105–107]. Raman is generally used for the study of the carbon component in terms of structure (crystalline vs. amorphous), defect levels, crystallites size, changes upon lithiation, etc. also allowing for spatial resolution (microRaman setups). EELS, which exploits the inelastic scattering of electrons (typically provided by TEM) from the sample, gives information about chemical composition and structure down to the atomic level.

Recently, nuclear magnetic resonance (NMR) was also exploited for the in-situ investigation of LIBs, thanks to the introduction of high-resolution solid-state techniques,

sequences for the investigation of paramagnetic compounds, and (micro)imaging methods (magnetic resonance imaging or MRI) [38,39,108–111]. NMR offers nuclear selectivity, and the different interactions (magnetic dipolar, electric quadrupolar, chemical shift anisotropy) can be exploited to better characterize the different components in the electrode and electrolyte. Recently, NMR has been exploited for the study of interfaces, thanks to dynamic nuclear polarization (DNP) and imaging techniques [112,113].

Other spectroscopic techniques, such as mass spectrometry, MS, [114], Mössbauer spectroscopy [115], and electron paramagnetic resonance, EPR, [116] have been exploited. For a systematic classification and discussion on the state-of-the-art techniques and available procedures for interface/interphase analysis it is possible to refer to dedicated reviews [117–119].

Finally, the investigation of interfaces/interphases can be carried out with the help of advanced electrochemical techniques, including: (i) electrochemical acoustic analysis [120–122]; (ii) quartz crystal microbalance, EQCM, [123,124]; (iii) electrochemical impedance spectroscopy, EIS, [125], and (iv) scanning electrochemical microscopy [126].

Table 1. Pros and cons of some characterization techniques of interest for lithium batteries. A: spatial resolution; B: temporal resolution/acquisition speed; C: structure/phase selectivity; D: chemical selectivity; E: sensitivity; F: setup complexity; G: in-situ/*operando* capabilities; H: cost/accessibility. Five levels scale: ++, +, =, -, -. N.A.: not applicable/not relevant. See text for acronyms.

Technique	Ref.	A	B	C	D	E	F	G	H
RD	[27–34]	-	+	++	N.A.	+	=	-	++
Synch. Diff.	[29,30]	-	++	++	N.A.	++		++	-
Neutron diffr.	[35,37]	-	=	++	N.A.	=	-	+	-
XAS	[28,40–45]	-	+	+	+	+	-	-	-
XPS	[48–53]	-	+	=	++	+	-	-	-
Reflectometry	[54–58]	+	++	N.A.	N.A.	-	=	+	=
Opt. Micr.	[80,81]	-	+	N.A.	N.A.	-	+	-	++
SEM	[82,83]	+	=	+	++	++	-	-	+
TEM	[86–97]	++	+	++	+	++	-	-	-
AFM	[98–101]	++	=	=	N.A.	=	+	-	++
IR	[103,104]	=	-	-	++	-	++	-	++
Raman	[105–107]	+	-	-	++	-	+	-	+
NMR/MRI	[108–111]	=	-	=	++	-	-	=	=
XRT	[65–71]	++	++	++	N.A.	=	+	+	+
EIS	[125]	N.A.	-	N.A.	N.A.	N.A.	++	++	++

4. Future Developments

4.1. The Li/Electrolyte Interface

The intrinsic instability of the Li metal/electrolyte interface is the main obstacle towards the development of the lithium metal secondary battery (LMB) which is seen as one of the main breakthroughs in battery business. The implementation of a safe and reversible lithium plating/stripping process is carried on two development lines: (i) in the rocking chair configuration (lithiated cathode) it will be possible to develop a quasi-“lithium less” device, where the anode material is formed in-situ during the first charge, thus increasing the gravimetric energy, (ii) by using non-lithiated cathodes, overcoming the intrinsic limitation of intercalation chemistries and enabling the use of high capacity materials (S, O₂).

The presence of a SEI layer on the surface of metallic lithium is again a key point to improve electrolytes stability, since these latter work outside their thermodynamic electrochemical window. However, this scenario is completely different with respect to intercalation materials as graphite. The stripping/plating reaction takes place with a deep change of the electrode surface: fresh lithium is generated during plating and consumed during stripping. Thus, new SEI is formed during each plating cycle, with the corrosion of the metal active material, while the SEI fractures during stripping due to the generated mechanical strain. These processes have an opposite effect on the cell

stability/performances: the continuous growth of SEI in plating increases the interfacial impedance and thus the electrode overpotential, so affecting the rate capability of the material. At the same time, the fragility of the SEI during stripping boosts for the formation of lithium fractal structures (dendrites) in the next plating cycle, because the SEI microfractures become the space zone for fast development of such dendrites [127], which can propagate fast through the electrolyte, eventually giving internal short circuit and dramatic cell failures. Moreover, during the successive stripping, dendrites can be detached from the metal layer originating “death” lithium particles in the electrolyte.

The successful implementation of LMB passes through SEI stabilization, and several different strategies have been proposed so far (Figure 2) [128]. A first approach is the use of electrolyte additives to improve the SEI chemical and mechanical stability. One of the most investigated additives is LiNO_3 , because nitrates decompose around 1.7 V vs. Li^+/Li promoting the uniform growth of lithium during plating [129]. Moreover, the addition of polysulfide increases the homogeneity of the fresh metal layer [130]. Other investigated additives are FEC [131], AlI_3 [132], and Cs salts to promote the electrostatic shield mechanisms [133].

A second way to improve the interfacial properties of the $\text{Li}/\text{electrolyte}$ interphase is the pretreatment of the metal to produce an artificial SEI layer before assembling the cell. From the interfacial point of view, there are two possibilities in this regard: to build the artificial layer onto the Cu current collector and to use it as a scaffold for the plating of lithium, or to make the SEI directly on the lithium foil. The former approach was used with porous carbonaceous materials such as carbon nanospheres [134], or 2D materials as boron nitride and graphene [135]. During plating, lithium ions can penetrate the layer and the lithium is deposited between the artificial SEI and the Cu foil. These SEIs show better mechanical and chemical properties compared to layers formed onto the lithium foil by electrolyte decomposition, increasing the Coulomb efficiency and the lifetime of the lithium anodes. Similar results were obtained with a series of protective layers of inorganic (LiF , Li_3N , LiPO_4 , Al_2O_3) and organic (NafionTM, polyacrylic acid, polyacetylene) materials directly attached on the top of the lithium foil. Lithium-containing inorganic salts can be produced by the reaction of gases on the surface of metallic lithium (freon or F_2 for LiF [136,137], N_2 for Li_3N), or by chemical reactions in solution (CuF_2 for LiF [138]). The deposition of oxides can be performed by atomic layer deposition (ALD) [139]. In the case of organic materials, different strategies can be used to realize the protective layer: it can be laminated on the top, as in the case of a few μm NafionTM soaked with a commercial electrolyte [140], directed formed by the chemical reaction between the polyacrylic acid and Li [141] or by the in-situ polymerization to obtain conducting polymers (polyacetylene) [142].

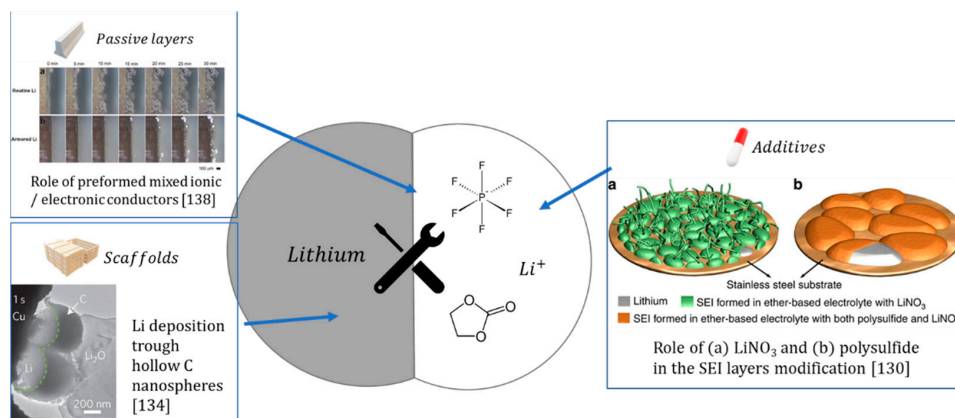


Figure 2. Examples of the different approaches to improve the interfacial properties of the $\text{Li}/\text{electrolyte}$ [138]. panel (a) taken from [134]; panel (b) taken from [130].

4.2. Beyond Graphite: Alloys for Negative Electrodes

High-capacity novel negative electrodes for LIBs include materials such as conversions oxides (SnO_2 , SiO_x) or metalloid elements (Si, Sn) able to make alloys with lithium. Despite of the obvious chemical differences between the two classes, their working principle in LIBs is similar, since MO_n oxides are converted to $\text{M}/\text{Li}_2\text{O}$ composites during the first cathodic reaction and then the reversible alligation reaction takes place:



Thus, in both cases, during cell functioning we should take in consideration the SEI layers on the metalloid surface, also because the conversion reactions take place at potentials often higher than the electrolyte decomposition one. These SEIs have similar problems as in the LMB case, i.e., mechanical instability due to the large volume changes during alloying and de-alloying, making the mechanisms of SEI formation dynamic and thus affecting the Coulomb efficiency of the process. The most important example in this regard is the use of silicon, beside lithium the material with the highest theoretical capacity for Li ions storage, thanks to the possibility to make alloys up to $\text{Li}_{4.4}\text{Si}$ and observed specific capacity exceeding 3500 mAh g^{-1} .

Studies for the implementation of silicon-based negative electrodes initially focused on the preparation of nanostructures able to allocate volume changes during alloying and de-alloying reactions, while neglecting the chemical aspects at the surfaces. The result was the preparation of high specific capacity electrodes with low efficiencies ($<99.5\%$) and therefore insufficient cycling capabilities [143], so the importance of the study and control of the interface has re-emerged. The earlier works on the nature of SEI layers on Si nanostructures revealed its chemical composition, made by LiF , Li_2CO_3 , LiSiO_x and organic compounds [144], as well as its dynamic nature, i.e., the SEI changes with the potential and the cycling [145]. One of the most promising ways to overcome this issue is to have a “non-filling” coating wrapping the porous silicon structures [146]. The non-filling coating is made by a carbon film able to form a stable SEI allowing the penetration of lithium ions in the ensemble of the porous nanoparticles, wherein they can expand and contract without mechanical damaging. The same approach was used in the case of micrometric pomegranate-shaped silicon particles covered by a thin layer of carbon [147]. With these systems, the life of silicon anodes was extended over 1000 cycles at high current density and a gravimetric capacity higher than 1000 mAh g^{-1} (Figure 3).

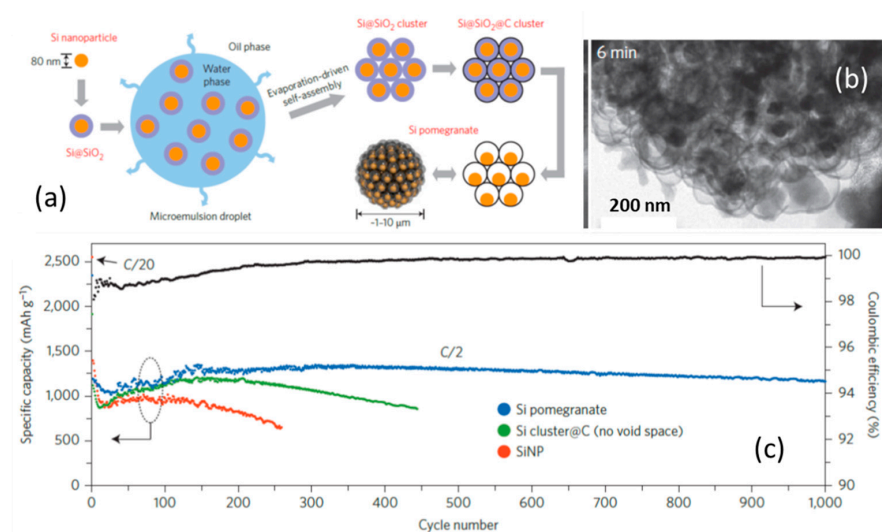


Figure 3. Use of carbon/silicon pomegranate morphologies. (a) Pomegranate preparation from core shell SiO_2/Si particles; (b) in-situ TEM image of the pomegranate particles under lithiation; (c) electrochemical performance of the pomegranate compared with silicon nanoparticles and core shell C/Si nano composite without void space. From reference [147].

4.3. Towards High Voltage: The Emerging Role of the CEI

LIB positive electrodes work at potentials just below the oxidative decomposition potential of the electrolyte, thus the role of the CEI interphase between the cathode and the electrolyte is often undervalued. However, in the last years, it emerged as one of the improving fields to design high energy materials, as well as more sustainable processes in battery manufacturing. Indeed, the attempts to produce high-capacity positive materials are not just focused in increasing the capacity, which is limited by the intercalation reaction, but also in enabling the use of high potential phases, such as the high voltage, Ni-based spinels ($\text{LiNi}_{0.5}\text{Mn}_{1.5}\text{O}_4$, LNMO) or olivines (LiCoPO_4) [148,149]. Moreover, the stability of Ni-rich materials (both layered oxides and spinels) in water is affected by corrosion with loss of the transition metal cation, a problem which is limiting the development of water-based procedure to formulate the electrode layers. Contrary to the graphite, indeed, the commercial processing of the cathode still requires the use of toxic 1-methyl-2-pyrrolidone (NMP).

One of the most interesting compounds, the spinel $\text{LiNi}_{0.5}\text{Mn}_{1.5}\text{O}_4$, has a plateau at 4.7 V vs. Li^+/Li , which is above the decomposition limit and leads to the formation of CEI. Apart the stabilization of the bulk structure of the spinel, proper surface engineering can be used to control the interphase between the active material particles and the electrolyte [150]. Seminal works on the properties of the $\text{LiNi}_{0.5}\text{Mn}_{1.5}\text{O}_4$ /electrolyte interface highlighted that its stability depends on crystal orientation, cations surface distribution, and surface reconstruction upon cycling [151,152]. The two main strategies to improve the interfacial properties are: (i) the coating of the active particles, and (ii) the use of electrolyte additives (see Figure 4). In the former case, a core-shell approach is applied to avoid the dissolution of transition metal cations and to inhibit the reaction with the electrolyte [153]. The proposed shells are usually made by ZnO , TiO_2 , or Al_2O_3 as nano-shells formed by chemical self-assembling [154] or ALD [155,156]. From the other part, a better design of the electrolytes can also enable the reversible operation of high voltage-spinel [157]. CEI-forming additives include: (i) phosphorous based compounds like (trimethylsilyl)phosphate [158], which exhibit higher HOMO energy and thus higher decomposition potentials, (ii) carbonyl molecules, like quercetin [159]; (iii) nitrile containing systems [160]), or different lithium salts and lithium borates [161,162]. Another possibility is to design electrolytes with high antioxidative ability, such as sulfone-based solutions [163], phosphate-based systems [164], fluorinated solvents [165], ionic liquids [166], and highly concentrated solutions [167].

Among the various cathode materials for future LIB generations, however, the most promising and investigated compounds in recent years have been the layered oxides of general composition $\text{LiNi}_x\text{Mn}_y\text{Co}_z\text{O}_2$ (NMCXYZ). The general trend in the composition optimization towards higher energy and low cost is the increase of the Ni amount with respect to the more toxic Co, also because of the better electrochemical properties of the couple $\text{Ni}^{4+}/\text{Ni}^{3+}$ compared to $\text{Co}^{4+}/\text{Co}^{3+}$. Thus, NMC evolution moved from NMC111 to NMC532 and NMC622 of the last commercial generation, aiming towards NMC811 which should be the cathode of the next LIBs. However, this comes with the increase of both the thermal instability and the solubility of the phase, affecting the capacity retention and inhibiting the processing in aqueous solution [168]. An intriguing solution to this problem is the active material surface control, with the preparation of microparticles of active material with a concentration gradient, which has an excess of Mn and Ni at the surface and in the bulk, respectively [169]. Despite of the presence of 80% on Ni in the phase, electrodes based on this kind of NMC811 showed better cyclability compared to the more stable bulk phase NMA [170].

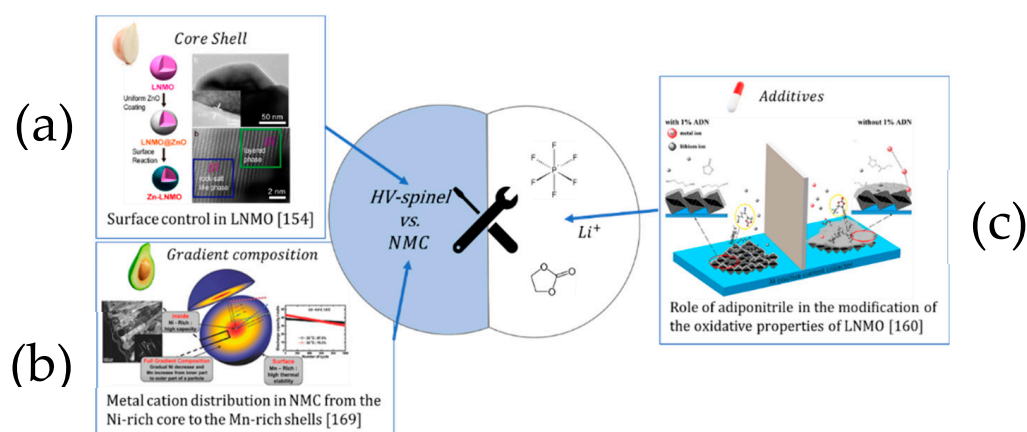


Figure 4. Examples of the different approaches to improve the properties of the positive electrode/electrolyte interface in LIBs. Panel (a) taken from [154]; panel (b) taken from ref. [169]; panel (c) taken from [160].

Finally, we mention that, in the case of CEI, the large molar amount of carbon additives used in electrode formulation has an important role in the decomposition of the electrolytes at high voltage, due to their nanometric size and good electrocatalytic activity, which is at least comparable with that of active oxides [171], without considering that carbon black with graphitic domains can intercalate anions at high voltage.

5. Conclusions

Extended interphases play an increasingly important role in determining the functional properties of electrochemical storage devices, especially regarding the long-term performance stability. While in the past decade the attention was focused on the graphite anode (SEI), the most recent technological developments place at the center of attention the interphase between the lithium metal and the electrolyte (liquid or solid), and CEI. Indeed, the advances in instrumentation setups and cell design allow for the implementation of in-situ and operando approaches of increasing complexity. This will help to understand the reaction mechanisms and to develop more sophisticated approaches for interphases design and control. At the same time, due to the complexity of the considered systems, SEI and CEI, it is not possible to identify a single technique of choice for the investigation of the battery interphases and multi-technique approaches should be preferred.

Author Contributions: C.F. developed the section on characterization techniques; R.R. developed the section of battery interphases; P.M. followed introduction and conclusions, and the overall organization of the paper. All authors have read and agreed to the published version of the manuscript.

Funding: This research was funded by Italian Ministry of Foreign Affairs under project ENVIRONMENTALIST. This research was also funded by Italian MIUR with the grant “Dipartimenti di Eccellenza–2017 “Materials For Energy”.

Institutional Review Board Statement: Not applicable.

Informed Consent Statement: Not applicable.

Data Availability Statement: Not applicable.

Conflicts of Interest: The authors declare no conflict of interest.

List of the Acronyms Used in the Text

AFM	Atomic Force Microscopy
ALD	Atomic Layer Deposition
CEI	Cathode Electrolyte Interphase
CEM	Cryogenic Electron Microscopy
DNP	Dynamic Nuclear Polarization
EC	Ethylene Carbonate
EELS	Electron Energy Loss Spectroscopy
EIS	Electrochemical Impedance Spectroscopy
EPR	Electron Paramagnetic Resonance
EQCM	Electrochemical Quartz Crystal Microbalance
FEC	Fluoroethylene Carbonate
FTIR	Fourier Transform Infrared spectroscopy
HOMO	Highest Occupied Molecular Orbital
INS	Inelastic Neutron Scattering
LIB	Lithium-Ion Battery
LMB	Lithium Metal Battery
LNMO	$\text{LiNi}_{0.5}\text{Mn}_{1.5}\text{O}_4$
MRI	Magnetic Resonance Imaging
MS	Mass Spectroscopy
NDP	Neutron Depth Profiling
NMA	Nickel-Manganese-Aluminum oxide
NMCXYZ	$\text{LiNi}_x\text{Mn}_y\text{Co}_z\text{O}_2$
NMP	1-methyl-2-pyrrolidone
NMR	Nuclear Magnetic Resonance
OM	Optical Microscopy
PC	Propylene Carbonate
PDF	Pair Distribution Function
PEO	Poly(ethylene oxide)
SANS	Small Angle Neutron Scattering
SECM	Scanning ElectroChemical Microscopy
SEI	Solid Electrolyte Interphase
SEM	Scanning Electron Microscopy
TEM	Transmission Electron Microscopy
VC	Vinylene carbonate
XAS	X-rays Absorption Spectroscopy
XPS	X-rays Photoelectron Spectroscopy
XRD	X-rays Diffraction
XRR	X-rays Reflectometry
XRT	X-rays Tomography
XTM	X-rays Transmission Microscopy

References

1. Saubanère, M.; Filhol, J.-S.; Doublet, M.-L. Atomistic Modeling of Electrode Materials for Li-Ion Batteries: From Bulk to Interfaces. In *Physical Multiscale Modeling and Numerical Simulation of Electrochemical Devices for Energy Conversion and Storage*; Franco, A.A., Doublet, M.-L., Bessler, W.G., Eds.; Springer: London, UK, 2016; pp. 1–36.
2. Bard, A.J.; Faulkner, L.R. *Electrochemical Methods, Fundamentals and Applications*, 2nd ed.; Wiley: New York, NY, USA, 2001.
3. Trasatti, S.; Parsons, R. Interphases in systems of conducting phases (IUPAC Recommendations 1985). *Pure Appl. Chem.* **1986**, *58*, 437–454. [CrossRef]
4. Advanced Materials for Clean and Sustainable Energy and Mobility. Available online: [https://emiri.eu/uploads/content_files/65/value__file/EMIRI%20Technology%20Roadmap%20-%20September%202019%20\(cond\).pdf](https://emiri.eu/uploads/content_files/65/value__file/EMIRI%20Technology%20Roadmap%20-%20September%202019%20(cond).pdf) (accessed on 23 February 2021).
5. Peled, E. The Electrochemical Behavior of Alkali and Alkaline Earth Metals in Nonaqueous Battery Systems—The Solid Electrolyte Interphase Model. *J. Electrochem. Soc.* **1979**, *126*, 2047–2051. [CrossRef]
6. Gauthier, M.A.M.; Carney, T.J.; Grimaud, A.; Giordano, L.; Pour, N.; Chang, H.-H.; Fenning, D.P.; Lux, S.F.; Paschos, O.; Bauer, C.; et al. Electrode–Electrolyte Interface in Li-Ion Batteries: Current Understanding and New Insights. *J. Phys. Chem. Lett.* **2015**, *6*, 4653–4672. [CrossRef] [PubMed]

7. Tan, S.; Ji, Y.J.; Zhang, Z.R.; Yang, Y. Recent Progress in Research on High-Voltage Electrolytes for Lithium-Ion Batteries. *ChemPhysChem* **2014**, *15*, 1956–1969. [[CrossRef](#)] [[PubMed](#)]
8. Kazzazi, A.; Bresser, D.; Kuenzel, M.; Hekmatfar, M.; Schnaidt, J.; Jusys, Z.; Diemant, T.; Behm, R.; Copley, M.; Maranski, K.; et al. Synergistic electrolyte additives for enhancing the performance of high-voltage lithium-ion cathodes in half-cells and full-cells. *J. Power Sources* **2021**, *482*, 228975. [[CrossRef](#)]
9. Asenbauer, J.; Eisenmann, T.; Kuenzel, M.; Kazzazi, A.; Chen, Z.; Bresser, D. The success story of graphite as a lithium-ion anode material—Fundamentals, remaining challenges, and recent developments including silicon (oxide) composites. *Sustain. Energy Fuels* **2020**, *4*, 5387–5416. [[CrossRef](#)]
10. Guerard, D.; Herold, A. Intercalation of lithium into graphite and other carbons. *Carbon* **1975**, *13*, 337–345. [[CrossRef](#)]
11. Dey, A.N.; Sullivan, B.P. The Electrochemical Decomposition of Propylene Carbonate on Graphite. *J. Electrochem. Soc.* **1970**, *117*, 222–224. [[CrossRef](#)]
12. Yazami, R.; Touzain, P. A reversible graphite-lithium negative electrode for electrochemical generators. *J. Power Sources* **1983**, *9*, 365–371. [[CrossRef](#)]
13. Fong, R.; Von Sacken, U.; Dahn, J.R. Studies of Lithium Intercalation into Carbons Using Nonaqueous Electrochemical Cells. *J. Electrochem. Soc.* **1990**, *137*, 2009–2013. [[CrossRef](#)]
14. Yoshino, A.; Sanechika, K.; Nakajima, T. Secondary Battery. U.S. Patent 4,668,595A, 26 May 1987.
15. Yoshino, A. *Lithium Ion Batteries*; Pistoia, G., Ed.; Elsevier: Amsterdam, The Netherlands, 2014.
16. Guyomard, D.; Tarascon, J.M. Rechargeable $\text{Li}_{1+x}\text{Mn}_2\text{O}_4/\text{Carbon}$ Cells with a New Electrolyte Composition: Potentiostatic Studies and Application to Practical Cells. *J. Electrochem. Soc.* **1993**, *140*, 3071–3081. [[CrossRef](#)]
17. Xu, K. Electrolytes and Interphases in Li-Ion Batteries and Beyond. *Chem. Rev.* **2014**, *114*, 11503–11618. [[CrossRef](#)] [[PubMed](#)]
18. Peled, E.; Menkin, S. Review—SEI: Past, Present and Future. *J. Electrochem. Soc.* **2017**, *164*, A1703–A1719. [[CrossRef](#)]
19. Shkrob, I.A.; Zhu, Y.; Marin, T.W.; Abraham, D. Reduction of Carbonate Electrolytes and the Formation of Solid-Electrolyte Interface (SEI) in Lithium-Ion Batteries. 1. Spectroscopic Observations of Radical Intermediates Generated in One-Electron Reduction of Carbonates. *J. Phys. Chem. C* **2013**, *117*, 19255–19269. [[CrossRef](#)]
20. Shkrob, I.A.; Zhu, Y.; Marin, T.W.; Abraham, D. Reduction of Carbonate Electrolytes and the Formation of Solid-Electrolyte Interface (SEI) in Lithium-Ion Batteries. 2. Radiolytically Induced Polymerization of Ethylene Carbonate. *J. Phys. Chem. C* **2013**, *117*, 19270–19279. [[CrossRef](#)]
21. Peled, E.; Bar Tow, D.; Merson, A.; Burnstein, L. Microphase structure of SEI on HOPG. *J. New Mater. Electrochem. Syst.* **2000**, *3*, 321–328.
22. Jeong, S.-K.; Inaba, M.; Abe, T.; Ogumi, Z. Surface Film Formation on Graphite Negative Electrode in Lithium-Ion Batteries: AFM Study in an Ethylene Carbonate-Based Solution. *J. Electrochem. Soc.* **2001**, *148*, A989–A993. [[CrossRef](#)]
23. Domi, Y.; Ochida, M.; Tsubouchi, S.; Nakagawa, H.; Yamanaka, T.; Doi, T.; Abe, T.; Ogumi, Z. In Situ AFM Study of Surface Film Formation on the Edge Plane of HOPG in Lithium-Ion Batteries. *ECS Meet. Abstr.* **2011**, *115*, 2548–25489. [[CrossRef](#)]
24. Schmitz, R.W.; Murmann, P.; Schmitz, R.; Müller, R.; Krämer, L.; Kasnatscheew, J.; Isken, P.; Niehoff, P.; Nowak, S.; Rösenthaller, G.-V.; et al. Investigations on novel electrolytes, solvents and SEI additives for use in lithium-ion batteries: Systematic electrochemical characterization and detailed analysis by spectroscopic methods. *Prog. Solid State Chem.* **2014**, *42*, 65–84. [[CrossRef](#)]
25. Santner, H.J.; Korepp, C.; Winter, M.; Besenhard, J.O. In-situ FTIR investigations on the reduction of vinylene electrolyte additives suitable for use in lithium-ion batteries. *Anal. Bioanal. Chem.* **2004**, *379*, 266–271. [[CrossRef](#)] [[PubMed](#)]
26. McMillan, R.; Slegel, H.; Shu, Z.X.; Wang, W. Fluoroethylene carbonate electrolyte and its use in lithium ion batteries with graphite anodes. *J. Power Sources* **1999**, *81–82*, 20–26. [[CrossRef](#)]
27. Shen, Y.; Pedersen, E.E.; Christensen, M.; Iversen, B.B. An electrochemical cell for in operando studies of lithium/sodium batteries using a conventional x-ray powder diffractometer. *Rev. Sci. Instrum.* **2014**, *85*, 104103. [[CrossRef](#)]
28. Silberstein, K.E.; Lowe, M.A.; Richards, B.; Gao, J.; Hanrath, T.; Abruña, H.D. Operando X-ray Scattering and Spectroscopic Analysis of Germanium Nanowire Anodes in Lithium Ion Batteries. *Langmuir* **2015**, *31*, 2028–2035. [[CrossRef](#)]
29. Arthur, Z.N.; Chiu, H.-C.; Lu, X.; Chen, N.; Emond, V.; Demopoulos, G.P.; Jiang, D.-T. In Operando XANES & XRD Investigation into the Rate-Dependent Transport Properties of Lithium Iron Silicate Cathodes. *MRS Adv.* **2017**, *2*, 419–424. [[CrossRef](#)]
30. Alemu, T.; Wang, F.-M. In situ electrochemical synchrotron radiation for Li ion batteries. *J. Synchrotron. Radiat.* **2018**, *25*, 151–165. [[CrossRef](#)] [[PubMed](#)]
31. Zhang, X.; Van Hulzen, M.; Singh, D.P.; Brownrigg, A.; Wright, J.P.; Van Dijk, N.H.; Wagemaker, M. Direct view on the phase evolution in individual LiFePO_4 nanoparticles during Li-ion battery cycling. *Nat. Commun.* **2015**, *6*, 8333. [[CrossRef](#)]
32. Chattopadhyay, S.; Lipson, A.L.; Karmel, H.J.; Emery, J.D.; Fister, T.T.; Fenter, P.A.; Hersam, M.C.; Bedzyk, M.J. In Situ X-ray Study of the Solid Electrolyte Interphase (SEI) Formation on Graphene as a Model Li-ion Battery Anode. *Chem. Mater.* **2012**, *24*, 3038–3043. [[CrossRef](#)]
33. Wagner, M.R.; Albering, J.H.; Moeller, K.-C.; Besenhard, J.O.; Winter, M. XRD evidence for the electrochemical formation of $\text{Li}+(\text{PC})_y\text{Cn-}$ in PC-based electrolytes. *Electrochem. Commun.* **2005**, *7*, 947–952. [[CrossRef](#)]
34. Buchberger, I.; Seidlmayer, S.; Pokharel, A.; Piana, M.; Hattendorff, J.; Kudejova, P.; Gilles, R.; Gasteiger, H.A. Aging analysis of graphite/ $\text{LiNi}_{1/3}\text{Mn}_{1/3}\text{Co}_{1/3}\text{O}_2$ cells using XRD, PGAA, and AC impedance. *J. Electrochem. Soc.* **2015**, *162*, A2737. [[CrossRef](#)]

35. Bianchini, M.; Leriche, J.B.; Laborier, J.-L.; Gendrin, L.; Suard, E.; Croguennec, L.; Masquelier, C. A New Null Matrix Electrochemical Cell for Rietveld Refinements of In-Situ or Operando Neutron Powder Diffraction Data. *J. Electrochem. Soc.* **2013**, *160*, A2176–A2183. [\[CrossRef\]](#)
36. Boulet-Roblin, L.; Borel, P.; Sheptyakov, D.; Tessier, C.; Novák, P.; Villevieille, C. Operando Neutron Powder Diffraction Using Cylindrical Cell Design: The Case of $\text{LiNi}_{0.5}\text{Mn}_{1.5}\text{O}_4$ vs Graphite. *J. Phys. Chem. C* **2016**, *120*, 17268–17273. [\[CrossRef\]](#)
37. Shiotani, S.; Naka, T.; Morishima, M.; Yonemura, M.; Kamiyama, T.; Ishikawa, Y.; Ukyo, Y.; Uchimoto, Y.; Ogumi, Z. Degradation analysis of 18650-type lithium-ion cells by operando neutron diffraction. *J. Power Sources* **2016**, *325*, 404–409. [\[CrossRef\]](#)
38. Key, B.; Morcrette, M.; Tarascon, J.-M.; Grey, C.P. Pair Distribution Function Analysis and Solid State NMR Studies of Silicon Electrodes for Lithium Ion Batteries: Understanding the (De)lithiation Mechanisms. *J. Am. Chem. Soc.* **2011**, *133*, 503–512. [\[CrossRef\]](#) [\[PubMed\]](#)
39. Allan, P.K.; Griffin, J.M.; Darwiche, A.; Borkiewicz, O.J.; Wiaderek, K.M.; Chapman, K.W.; Morris, A.J.; Chupas, P.J.; Monconduit, L.; Grey, C.P. Tracking Sodium-Antimonide Phase Transformations in Sodium-Ion Anodes: Insights from Operando Pair Distribution Function Analysis and Solid-State NMR Spectroscopy. *J. Am. Chem. Soc.* **2016**, *138*, 2352–2365. [\[CrossRef\]](#)
40. Khalid, S.; Caliebe, W.; Siddons, P.; So, I.; Clay, B.; Lenhard, T.; Hanson, J.; Wang, Q.; Frenkel, A.; Marinkovic, N.; et al. Quick extended x-ray absorption fine structure instrument with millisecond time scale, optimized for in situ applications. *Rev. Sci. Instrum.* **2010**, *81*, 15105. [\[CrossRef\]](#)
41. Li, C.; Sarapulova, A.; Pfeifer, K.; Luo, X.; Casati, N.P.M.; Welter, E.; Melinte, G.; Fu, Q.; Dsoke, S. Elucidating the Mechanism of Li Insertion into Fe1-xS/Carbon via In Operando Synchrotron Studies. *ACS Appl. Mater. Interfaces* **2020**, *12*, 52691–52700. [\[CrossRef\]](#)
42. Dixon, D.; Ávila, M.; Ehrenberg, H.; Bhaskar, A. Difference in Electrochemical Mechanism of SnO_2 Conversion in Lithium-Ion and Sodium-Ion Batteries: Combined in Operando and Ex Situ XAS Investigations. *ACS Omega* **2019**, *4*, 9731–9738. [\[CrossRef\]](#)
43. Deng, S.; Sun, Q.; Li, M.; Adair, K.; Yu, C.; Li, J.; Li, W.; Fu, J.; Li, X.; Li, R.; et al. Insight into cathode surface to boost the performance of solid-state batteries. *Energy Storage Mater.* **2021**, *35*, 661–668. [\[CrossRef\]](#)
44. Bleith, P.; van Beek, W.; Kaiser, H.; Novak, P.; Villevieille, C. Simultaneous in situ X-ray absorption spectroscopy and X ray diffraction studies on battery materials: The case of $\text{Fe}_{0.5}\text{TiOPO}_4$. *J. Phys. Chem C* **2015**, *119*, 3466–3471. [\[CrossRef\]](#)
45. Arthur, Z.; Chiu, H.-C.; Lu, X.; Chen, N.; Emond, V.; Zaghib, K.; Jiang, D.-T.; Demopoulos, G.P. Spontaneous reaction between an uncharged lithium iron silicate cathode and a LiPF_6 -based electrolyte. *Chem. Commun.* **2015**, *52*, 190–193. [\[CrossRef\]](#) [\[PubMed\]](#)
46. Yamamoto, K.; Orikasa, Y.; Takamatsu, D.; Koyama, Y.; Mori, S.; Masese, T.; Mori, T.; Minato, T.; Tanida, H.; Uruga, T.; et al. Stabilization of the Electronic Structure at the Cathode/Electrolyte Interface via MgO Ultra-thin Layer during Lithium-ions Insertion/Extraction. *Electrochemistry* **2014**, *82*, 891–896. [\[CrossRef\]](#)
47. Wandt, J.; Freiberg, A.; Thomas, R.; Gorlin, Y.; Siebel, A.; Jung, R.; Gasteiger, H.A.; Tromp, M. Transition metal dissolution and deposition in Li-ion batteries investigated by operando X-ray absorption spectroscopy. *J. Mater. Chem. A* **2016**, *4*, 18300–18305. [\[CrossRef\]](#)
48. Philippe, B.; Hahlin, M.; Edström, K.; Gustafsson, T.; Siegbahn, H.; Rensmo, H. Photoelectron Spectroscopy for Lithium Battery Interface Studies. *J. Electrochem. Soc.* **2015**, *163*, A178–A191. [\[CrossRef\]](#)
49. Verma, P.; Maire, P.; Novak, P. A review of the features and analysis of the solid electrolyte interphase in Li-ion batteries. *Electrochim. Acta* **2010**, *55*, 6332–6341. [\[CrossRef\]](#)
50. Cherkashinin, G.; Motzko, M.; Schulz, N.; Späth, T.; Jaegermann, W. Electron Spectroscopy Study of $\text{Li}[\text{Ni},\text{Co},\text{Mn}]\text{O}_2$ /Electrolyte Interface: Electronic Structure, Interface Composition, and Device Implications. *Chem. Mater.* **2015**, *27*, 2875–2887. [\[CrossRef\]](#)
51. Davis, A.L.; Garcia-Mendez, R.; Wood, K.N.; Kazyak, E.; Chen, K.-H.; Teeter, G.; Sakamoto, J.; Dasgupta, N.P. Electro-chemo-mechanical evolution of sulfide solid electrolyte/Li metal interfaces: Operando analysis and ALD interlayer effects. *J. Mater. Chem. A* **2020**, *8*, 6291–6302. [\[CrossRef\]](#)
52. Schwöbel, A.; Hausbrand, R.; Jaegermann, W. Interface reactions between LiPON and lithium studied by in-situ X-ray photoemission. *Solid State Ion.* **2015**, *273*, 51–54. [\[CrossRef\]](#)
53. Tang, C.-Y.; Haasch, R.T.; Dillon, S.J. In situ X-ray photoelectron and Auger electron spectroscopic characterization of reaction mechanisms during Li-ion cycling. *Chem. Commun.* **2016**, *52*, 13257–13260. [\[CrossRef\]](#)
54. Hirayama, M.; Sonoyama, N.; Abe, T.; Minoura, M.; Ito, M.; Mori, D.; Yamada, A.; Kanno, R.; Terashima, T.; Takano, M.; et al. Characterization of electrode/electrolyte interface for lithium batteries using in situ synchrotron X-ray reflectometry—A new experimental technique for LiCoO_2 model electrode. *J. Power Sources* **2007**, *168*, 493–500. [\[CrossRef\]](#)
55. Kawaguchi, T.; Shimada, K.; Ichitsubo, T.; Yagi, S.; Matsubara, E. Surface-layer formation by reductive decomposition of LiPF_6 at relatively high potentials on negative electrodes in lithium ion batteries and its suppression. *J. Power Sources* **2014**, *271*, 431–436. [\[CrossRef\]](#)
56. Jerliu, B.; Hüger, E.; Horisberger, M.; Stahn, J.; Schmidt, H. Irreversible lithium storage during lithiation of amorphous silicon thin film electrodes studied by in-situ neutron reflectometry. *J. Power Sources* **2017**, *359*, 415–421. [\[CrossRef\]](#)
57. Owejan, J.E.; Owejan, J.P.; Decaluwe, S.C.; Dura, J.A. Solid Electrolyte Interphase in Li-Ion Batteries: Evolving Structures Measured In situ by Neutron Reflectometry. *Chem. Mater.* **2012**, *24*, 2133–2140. [\[CrossRef\]](#)
58. Hirayama, M.; Yonemura, M.; Suzuki, K.; Torikai, N.; Smith, H.; Watkinsand, E.; Majewski, J.; Kanno, R. Surface Characterization of LiFePO_4 Epitaxial Thin Films by X-ray/Neutron Reflectometry. *Electrochemistry* **2010**, *78*, 413–415. [\[CrossRef\]](#)

59. Metwalli, E.; Götz, K.; Lages, S.; Bär, C.; Zech, T.; Noll, D.M.; Schuldes, I.; Schindler, T.; Prihoda, A.; Lang, H.; et al. A novel experimental approach for nanostructure analysis: Simultaneous small-angle X-ray and neutron scattering. *J. Appl. Crystallogr.* **2020**, *53*, 722–733. [\[CrossRef\]](#)
60. Hattendorff, J.; Seidlmayer, S.; Gasteiger, H.A.; Gilles, R. Li-ion half-cells studied operando during cycling by small-angle neutron scattering. *J. Appl. Crystallogr.* **2020**, *53*, 210–221. [\[CrossRef\]](#) [\[PubMed\]](#)
61. Paul, N.; Wetjen, M.; Busch, S.; Gasteiger, H.; Gilles, R. Contrast Matched SANS for Observing SEI and Pore Clogging in Silicon-Graphite Anodes. *J. Electrochem. Soc.* **2019**, *166*, A1051–A1054. [\[CrossRef\]](#)
62. Zhao, E.; Zhang, Z.-G.; Li, X.; He, L.; Yu, X.; Li, H.; Wang, F. Neutron-based characterization techniques for lithium-ion battery research. *Chin. Phys. B* **2020**, *29*, 018201. [\[CrossRef\]](#)
63. Sacci, R.L.; Bañuelos, J.L.; Veith, G.M.; Littrell, K.C.; Cheng, Y.Q.; Wildgruber, C.U.; Jones, L.L.; Ramirez-Cuesta, A.J.; Rother, G.; Dudney, N.J.; et al. Structure of Spontaneously Formed Solid-Electrolyte Interphase on Lithiated Graphite Determined Using Small-Angle Neutron Scattering. *J. Phys. Chem. C* **2015**, *119*, 9816–9823. [\[CrossRef\]](#)
64. Bridges, C.A.; Sun, X.-G.; Zhao, J.; Paranthaman, M.P.; Dai, S. In Situ Observation of Solid Electrolyte Interphase Formation in Ordered Mesoporous Hard Carbon by Small-Angle Neutron Scattering. *J. Phys. Chem. C* **2012**, *116*, 7701–7711. [\[CrossRef\]](#)
65. Holler, M.; Guizar-Sicairos, M.; Tsai, E.H.; Dinapoli, R.; Müller, E.; Bunk, O.; Aeppli, G. High-resolution non-destructive three-dimensional imaging of integrated circuits. *Nat. Cell Biol.* **2017**, *543*, 402–406. [\[CrossRef\]](#)
66. Heenan, T.M.; Tan, C.; Hack, J.; Brett, D.J.; Shearing, P.R. Developments in X-ray tomography characterization for electrochemical devices. *Mater. Today* **2019**, *31*, 69–85. [\[CrossRef\]](#)
67. Wang, L.; Wang, J.; Zuo, P. Probing Battery Electrochemistry with In Operando Synchrotron X-Ray Imaging Techniques. *Small Methods* **2018**, *2*, 1700293. [\[CrossRef\]](#)
68. Wolf, M.; May, B.M.; Cabana, J. Visualization of Electrochemical Reactions in Battery Materials with X-ray Microscopy and Mapping. *Chem. Mater.* **2017**, *29*, 3347–3362. [\[CrossRef\]](#)
69. Kimura, Y.; Tomura, A.; Fakkao, M.; Nakamura, T.; Ishiguro, N.; Sekizawa, O.; Nitta, K.; Uruga, T.; Okumura, T.; Tada, M.; et al. 3D Operando Imaging and Quantification of Inhomogeneous Electrochemical Reactions in Composite Battery Electrodes. *J. Phys. Chem. Lett.* **2020**, *11*, 3629–3636. [\[CrossRef\]](#) [\[PubMed\]](#)
70. Vanpeene, V.; Villanova, J.; Suuronen, J.-P.; King, A.; Bonnin, A.; Adrien, J.; Maire, E.; Roué, L. Monitoring the morphological changes of Si-based electrodes by X-ray computed tomography: A 4D-multiscale approach. *Nano Energy* **2020**, *74*, 104848. [\[CrossRef\]](#)
71. Ziesche, R.F.; Arlt, T.; Finegan, D.P.; Heenan, T.M.M.; Tengattini, A.; Baum, D.; Kardjilov, N.; Markötter, H.; Manke, I.; Kockelmann, W.; et al. 4D imaging of lithium-batteries using correlative neutron and X-ray tomography with a virtual unrolling technique. *Nat. Commun.* **2020**, *11*, 1–11. [\[CrossRef\]](#) [\[PubMed\]](#)
72. Kardjilov, N.; Manke, I.; Woracek, R.; Hilger, A.; Banhart, J. Advances in neutron imaging. *Mater. Today* **2018**, *21*, 652–672. [\[CrossRef\]](#)
73. Senyshyn, A.; Muhlbauer, M.J.; Nikolowski, K.; Pirling, T.; Ehrenberg, H. “In operando” neutron scattering studies on Li-ion batteries. *J. Power Sources* **2012**, *203*, 126–129. [\[CrossRef\]](#)
74. Butler, L.G.; Schillinger, B.; Ham, K.; Dobbins, T.A.; Liu, P.; Vajo, J.J. Neutron imaging of a commercial Li-ion battery during discharge: Application of monochromatic imaging and polychromatic dynamic tomography. *Nucl. Instrum. Methods Phys. Res. Sect. A* **2011**, *651*, 320–328. [\[CrossRef\]](#)
75. Goers, D.; Holzapfel, M.; Scheifele, W.; Lehmann, E.; Vontobel, P.; Novák, P. In situ neutron radiography of lithium-ion batteries: The gas evolution on graphite electrodes during the charging. *J. Power Sources* **2004**, *130*, 221–226. [\[CrossRef\]](#)
76. Lanz, M.; Lehmann, E.; Imhof, R.; Exnar, I.; Novák, P. In situ neutron radiography of lithium-ion batteries during charge/discharge cycling. *J. Power Sources* **2001**, *101*, 177–181. [\[CrossRef\]](#)
77. Goldner, R.B.; Haas, T.E.; Arntz, F.O.; Slaven, S.; Wong, K.K.; Wilkens, B.; Shepard, C.; Lanford, W. Nuclear reaction analysis profiling as direct evidence for lithium ion mass transport in thin film “rocking-chair” structures. *Appl. Phys. Lett.* **1993**, *62*, 1699–1701. [\[CrossRef\]](#)
78. Lamaze, G.P.; Chen-Mayer, H.; Badding, M.; Laby, L. In situ measurement of lithium movement in thin film electrochromic coating using cold neutron depth profiling. *Surf. Interface Anal.* **1999**, *27*, 644–647. [\[CrossRef\]](#)
79. Lamaze, G.; Chen-Mayer, H.; Becker, D.; Vereda, F.; Goldner, R.; Haas, T.; Zerigian, P. Cold neutron depth profiling of lithium-ion battery materials. *J. Power Sources* **2003**, *119–121*, 680–685. [\[CrossRef\]](#)
80. Brissot, C.; Rosso, M.; Chazalviel, J.-N.; Baudry, P.; Lascaud, S. In situ study of dendritic growth in lithium/PEO-salt/lithium cells. *Electrochim. Acta* **1998**, *43*, 1569–1574. [\[CrossRef\]](#)
81. Steiger, J.; Richter, G.; Wenk, M.; Kramer, D.; Mönig, R. Comparison of the growth of lithium filaments and dendrites under different conditions. *Electrochem. Commun.* **2015**, *50*, 11–14. [\[CrossRef\]](#)
82. Orsini, F.; Du Pasquier, A.; Beaudouin, B.; Tarascon, J.; Trentin, M.; Langenhuizen, N.; De Beer, E.; Notten, P. In situ SEM study of the interfaces in plastic lithium cells. *J. Power Sources* **1999**, *81–82*, 918–921. [\[CrossRef\]](#)
83. Wei, C.-Y.; Lee, P.-C.; Tsao, C.-W.; Lee, L.-H.; Wang, D.-Y.; Wen, C.-Y. In situ Scanning Electron Microscopy Observation of MoS₂ Nanosheets during Lithiation in Lithium Ion Batteries. *ACS Appl. Energy Mater.* **2020**, *3*, 7066–7072. [\[CrossRef\]](#)
84. Raimann, P.R.; Hochgatterer, N.S.; Korepp, C.; Moller, K.C.; Winter, M.; Schrottner, H.; Hofer, F.; Besenhard, J.O. Monitoring dynamics of electrode reactions in Li-ion batteries by in situ ESEM. *Ionics* **2006**, *12*, 253–255. [\[CrossRef\]](#)

85. Lee, S.-H.; You, H.-G.; Han, K.-S.; Kim, J.; Jung, I.-H.; Song, J.-H. A new approach to surface properties of solid electrolyte interphase on a graphite negative electrode. *J. Power Sources* **2014**, *247*, 307–313. [\[CrossRef\]](#)
86. Fan, Z.; Zhang, L.; Baumann, D.; Mei, L.; Yao, Y.; Duan, X.; Shi, Y.; Huang, J.; Huang, Y.; Duan, X. In Situ Transmission Electron Microscopy for Energy Materials and Devices. *Adv. Mater.* **2019**, *31*, e1900608. [\[CrossRef\]](#) [\[PubMed\]](#)
87. Li, J.; Johnson, G.; Zhang, S.; Su, D. In Situ Transmission Electron Microscopy for Energy Applications. *Joule* **2019**, *3*, 4–8. [\[CrossRef\]](#)
88. Basak, S.; Ganapathy, S.; Malladi, S.K.; Vicarelli, L.; Schreuders, H.; Dam, B.; Kelder, E.M.; Wagemaker, M.; Zandbergen, H.W. Designing Reliable Operando TEM Experiments to Study (De)lithiation Mechanism of Battery Electrodes. *J. Electrochem. Soc.* **2019**, *166*, A3384–A3386. [\[CrossRef\]](#)
89. Gong, C.; Pu, S.D.; Gao, X.; Yang, S.; Liu, J.; Ning, Z.; Rees, G.J.; Capone, I.; Pi, L.; Liu, B.; et al. Revealing the Role of Fluoride-Rich Battery Electrode Interphases by Operando Transmission Electron Microscopy. *Adv. Energy Mater.* **2021**, *11*, 2003118. [\[CrossRef\]](#)
90. Fawey, M.H.; Chakravadhanula, V.S.K.; Munnangi, A.R.; Rongeat, C.; Hahn, H.; Fitchner, M.; Kubler, C. First results from in situ transmission electron microscopy studies of all-solid-state fluoride ion batteries. *J. Power Sources* **2020**, *466*, 228283. [\[CrossRef\]](#)
91. Mu, X.; Mazilkin, A.; Sprau, C.; Colsmann, A.; Kübel, C. Mapping structure and morphology of amorphous organic thin films by 4D-STEM pair distribution function analysis. *Microscopy* **2019**, *68*, 301–309. [\[CrossRef\]](#)
92. Li, Z.; Tan, X.; Li, P.; Kalisvaart, P.; Janish, M.T.; Mook, W.M.; Lubner, E.J.; Jungjohann, K.L.; Carter, C.B.; Mitlin, D. Coupling in Situ TEM and Ex Situ Analysis to Understand Heterogeneous Sodiation of Antimony. *Nano Lett.* **2015**, *15*, 6339–6348. [\[CrossRef\]](#) [\[PubMed\]](#)
93. Liu, X.H.; Huang, J.Y. In situ TEM electrochemistry of anode materials in lithium ion batteries. *Energy Environ. Sci.* **2011**, *4*, 3844–3860. [\[CrossRef\]](#)
94. Huang, J.Y.; Zhong, L.; Wang, C.M.; Sullivan, J.P.; Xu, W.; Zhang, L.Q.; Mao, S.X.; Hudak, N.S.; Liu, X.H.; Subramanian, A.; et al. In Situ Observation of the Electrochemical Lithiation of a Single SnO₂ Nanowire Electrode. *Science* **2010**, *330*, 1515–1520. [\[CrossRef\]](#)
95. Sacci, R.L.; Dudney, N.J.; More, K.L.; Parent, L.R.; Arslan, I.; Browning, N.D.; Unocic, R.R. Direct visualization of initial SEI morphology and growth kinetics during lithium deposition by in situ electrochemical transmission electron microscopy. *Chem. Commun.* **2014**, *50*, 2104–2107. [\[CrossRef\]](#) [\[PubMed\]](#)
96. Zeng, X.; Liu, D.; Wang, S.; Liu, S.; Cai, X.; Zhang, L.; Zhao, R.; Li, B.; Kang, F. In Situ Observation of Interface Evolution on a Graphite Anode by Scanning Electrochemical Microscopy. *ACS Appl. Mater. Interfaces* **2020**, *12*, 37047–37053. [\[CrossRef\]](#)
97. Zhang, Z.; Yang, J.; Huang, W.; Wang, H.; Zhou, W.; Li, Y.; Li, Y.; Xu, J.; Huang, W.; Chiu, W.; et al. Cathode-Electrolyte Interphase in Lithium Batteries Revealed by Cryogenic Electron Microscopy. *Matter* **2021**, *4*, 302–312. [\[CrossRef\]](#)
98. Aurbach, D.; Cohen, Y. The Application of Atomic Force Microscopy for the Study of Li Deposition Processes. *J. Electrochem. Soc.* **1996**, *143*, 3525–3532. [\[CrossRef\]](#)
99. Edstrom, K.; Herranen, M. Thermal Stability of the HOPG/Liquid Electrolyte Interphase Studied by In Situ Electrochemical Atomic Force Microscopy. *J. Electrochem. Soc.* **2000**, *147*, 3628–3632. [\[CrossRef\]](#)
100. Jiang, C.-S.; Yin, Y.; Guthrey, H.; Park, K.; Lee, S.-H.; Al-Jassim, M. Local electrical degradations of solid-state electrolyte by nm-scale operando imaging of ionic and electronic transports. *J. Power Sources* **2021**, *481*, 229138. [\[CrossRef\]](#)
101. Zhang, Z.; Smith, K.; Jervis, R.; Shearing, P.R.; Miller, T.S.; Brett, D.J.L. Operando Electrochemical Atomic Force Microscopy of Solid-Electrolyte Interphase Formation on Graphite Anodes: The Evolution of SEI Morphology and Mechanical Properties. *ACS Appl. Mater. Interfaces* **2020**, *12*, 35132–35141. [\[CrossRef\]](#) [\[PubMed\]](#)
102. Novák, P.; Joho, F.; Lanz, M.; Rykard, B.; Panitz, J.-C.; Allia, D.; Kötz, R.; Haas, O. The complex electrochemistry of graphite electrodes in lithium-ion batteries. *J. Power Sources* **2001**, *97–98*, 39–46. [\[CrossRef\]](#)
103. Charles-Blin, Y.; Flahaut, D.; Guérin, K.; Dubois, M.; Monconduit, L.; Louvain, N.; Martinez, H. Surface atomic layer fluorination of Li₄Ti₅O₁₂: Investigation of the surface electrode reactivity and the outgassing behavior in LiBs. *Appl. Surf. Sci.* **2020**, *527*, 146834. [\[CrossRef\]](#)
104. Li, J.; Fang, J.; Su, H.; Sun, S. Interfacial processes of lithium ion batteries by FTIR spectroscopy. *Prog. Chem.* **2011**, *23*, 349–356.
105. Bhattacharya, S.; Reza Riahi, A.; Alpas, A.T. Electrochemical cycling behavior of lithium carbonate (Li₂CO₃) pre-treated graphite anodes-SEI formation and graphite damage mechanisms. *Carbon* **2014**, *77*, 99–112. [\[CrossRef\]](#)
106. Hy, S.; Felix, Chen, Y.-H.; Liu, J.-Y.; Rick, J.; Hwang, B.-J. In situ surface enhanced Raman spectroscopic studies of solid electrolyte interphase formation in lithium ion battery electrodes. *J. Power Sources* **2014**, *256*, 324–328. [\[CrossRef\]](#)
107. Odziemkowski, M.; Krell, M.; Irish, D.E. A Raman Microprobe in Situ and Ex Situ Study of Film Formation at Lithium/Organic Electrolyte Interfaces. *J. Electrochem. Soc.* **1992**, *139*, 3052–3063. [\[CrossRef\]](#)
108. Bhattacharyya, R.; Key, B.; Chen, H.; Best, A.S.; Hollenkamp, A.F.; Grey, C.P. In situ NMR observation of the formation of metallic lithium microstructures in lithium batteries. *Nat. Mater.* **2010**, *9*, 504–510. [\[CrossRef\]](#)
109. Hsieh, Y.-C.; Thienenkamp, J.H.; Huang, C.-J.; Tao, H.-C.; Rodehorst, U.; Hwang, B.J.; Winter, M.; Brunklaus, G. Revealing the Impact of Film-Forming Electrolyte Additives on Lithium Metal Batteries via Solid-State NMR/MRI Analysis. *J. Phys. Chem. C* **2021**, *125*, 252–265. [\[CrossRef\]](#)
110. Märker, K.; Xu, C.; Grey, C.P. Operando NMR of NMC811/Graphite Lithium-Ion Batteries: Structure, Dynamics, and Lithium Metal Deposition. *J. Am. Chem. Soc.* **2020**, *142*, 17447–17456. [\[CrossRef\]](#) [\[PubMed\]](#)

111. Mohammadi, M.; Jerschow, A. In situ and operando magnetic resonance imaging of electrochemical cells: A perspective. *J. Magn. Reson.* **2019**, *308*, 106600. [[CrossRef](#)] [[PubMed](#)]
112. Hope, M.A.; Rinkel, B.L.D.; Gunnarsdottir, A.B.; Marker, K.; Menkin, S.; Paul, S.; Sergeyev, I.V.; Grey, C.P. Selective NMR observation of the SEI-metal interface by dynamic nuclear polarization from lithium metal. *Nat. Commun.* **2020**, *11*, 2224. [[CrossRef](#)] [[PubMed](#)]
113. Xiang, Y.; Zheng, G.; Liang, Z.; Jin, Y.; Liu, X.; Chen, S.; Zhou, K.; Zhu, J.; Lin, M.; He, H.; et al. Visualizing the growth process of sodium microstructures in sodium batteries by in-situ ^{23}Na MRI and NMR spectroscopy. *Nat. Nanotechnol.* **2020**, *15*, 883–890. [[CrossRef](#)]
114. Zhou, Y.; Su, M.; Yu, X.; Zhang, Y.; Wang, J.-G.; Ren, X.; Cao, R.; Xu, W.; Baer, D.R.; Du, Y.; et al. Real-time mass spectrometric characterization of the solid–electrolyte interphase of a lithium-ion battery. *Nat. Nanotechnol.* **2020**, *15*, 224–230. [[CrossRef](#)]
115. Joshi, T.; Eom, K.; Yushin, G.; Fuller, T.F. Effects of Dissolved Transition Metals on the Electrochemical Performance and SEI Growth in Lithium-Ion Batteries. *J. Electrochem. Soc.* **2014**, *161*, A1915–A1921. [[CrossRef](#)]
116. GirishKumar, G.; Bailey, W.H.; Peterson, B.K.; Casteel, W.J. Electrochemical and spectroscopic investigation of the overcharge behavior of stable electrolyte salts in lithium-ion batteries. *J. Electrochem. Soc.* **2011**, *158*, A146–A153. [[CrossRef](#)]
117. Liu, W.; Liu, P.; Mitlin, D. Review of emerging concepts in SEI analysis and artificial SEI membranes for lithium, sodium, and potassium metal battery anodes. *Adv. Energy Mater.* **2020**, *10*, 2002297. [[CrossRef](#)]
118. Tripathi, A.M.; Su, W.-N.; Hwang, B.J. In situ analytical techniques for battery interface analysis. *Chem. Soc. Rev.* **2018**, *47*, 736–851. [[CrossRef](#)]
119. Wang, H.; Li, X.; Li, F.; Liu, X.; Yang, S.; Ma, J. Formation and modification of cathode electrolyte interphase: A mini review. *Electrochem. Commun.* **2021**, *122*, 106870. [[CrossRef](#)]
120. Bommier, C.; Chang, W.; Li, J.; Biswas, S.; Davies, G.; Nanda, J.; Steingart, D. Operando Acoustic Monitoring of SEI Formation and Long-Term Cycling in NMC/SiGr Composite Pouch Cells. *J. Electrochem. Soc.* **2020**, *167*, 020517. [[CrossRef](#)]
121. Chang, W.; Bommier, C.; Fair, T.; Yeung, J.; Patil, S.; Steingart, D. Understanding Adverse Effects of Temperature Shifts on Li-Ion Batteries: An Operando Acoustic Study. *J. Electrochem. Soc.* **2020**, *167*, 090503. [[CrossRef](#)]
122. Lemarié, Q.; Idrissi, H.; Maire, E.; Thivel, P.-X.; Alloin, F.; Roué, L. Impact of the binder nature on the morphological change of sulfur electrodes upon cycling investigated by in situ characterization methods. *J. Power Sources* **2020**, *477*, 228374. [[CrossRef](#)]
123. Liu, T.; Lin, L.; Bi, X.; Tian, L.; Yang, K.; Liu, J.; Li, M.; Chen, Z.; Lu, J.; Amine, K.; et al. In situ quantification of interphasial chemistry in Li-ion battery. *Nat. Nanotechnol.* **2019**, *14*, 50–56. [[CrossRef](#)] [[PubMed](#)]
124. Kitz, P.G.; Lacey, M.J.; Novák, P.; Berg, E.J. Operando investigation of the solid electrolyte interphase mechanical and transport properties formed from vinylene carbonate and fluoroethylene carbonate. *J. Power Sources* **2020**, *477*, 228567. [[CrossRef](#)]
125. Nangir, M.; Massoudi, A.; Teyebifard, S.A. Investigation of the lithium-ion depletion in the silicon-silicon carbide anode/electrolyte interface in lithium-ion battery via electrochemical impedance spectroscopy. *J. Electroanal. Chem.* **2020**, *872*, 114385. [[CrossRef](#)]
126. Ebejer, N.; Schnippering, M.; Colburn, A.W.; Edwards, M.A.; Unwin, P.R. Localized High Resolution Electrochemistry and Multifunctional Imaging: Scanning Electrochemical Cell Microscopy. *Anal. Chem.* **2010**, *82*, 9141–9145. [[CrossRef](#)] [[PubMed](#)]
127. Wu, B.; Lochala, J.; Taverne, T.; Xiao, J. The interplay between solid electrolyte interface (SEI) and dendritic lithium growth. *Nano Energy* **2017**, *40*, 34–41. [[CrossRef](#)]
128. Wang, H.; Liu, Y.; Li, Y.; Cui, Y. Lithium Metal Anode Materials Design: Interphase and Host. *Electrochem. Energy Rev.* **2019**, *2*, 509–517. [[CrossRef](#)]
129. Liu, Y.Y.; Lin, D.C.; Li, Y.Z.; Chen, G.; Nix, O.; Li, Y.; Cui, Y. Solubility-mediated sustained release enabling nitrate additive in carbonate electrolytes for stable lithium metal anode. *Nat. Commun.* **2018**, *9*, 3656. [[CrossRef](#)]
130. Li, W.Y.; Yao, H.B.; Yan, K.; Zheng, G.; Liang, Z.; Chiang, Y.-M.; Cui, Y. The synergetic effect of lithium polysulfide and lithium nitrate to prevent lithium dendrite growth. *Nat. Commun.* **2015**, *6*, 7436. [[CrossRef](#)]
131. Zhang, X.-Q.; Cheng, X.-B.; Chen, X.; Yan, C.; Zhang, Q. Fluoroethylene Carbonate Additives to Render Uniform Li Deposits in Lithium Metal Batteries. *Adv. Funct. Mater.* **2017**, *27*, 1605989. [[CrossRef](#)]
132. Ma, L.; Kim, M.S.; Archer, L.A. Stable Artificial Solid Electrolyte Interphases for Lithium Batteries. *Chem. Mater.* **2017**, *29*, 4181–4189. [[CrossRef](#)]
133. Ding, F.; Xu, W.; Graff, G.L.; Zhang, G.; Sushko, M.L.; Chen, X.; Shao, Y.; Engelhard, M.H.; Nie, Z.; Xiao, J.; et al. Dendrite-free lithium deposition via self-healing electrostatic shield mechanism. *J. Am. Chem. Soc.* **2013**, *135*, 4450–4456. [[CrossRef](#)]
134. Zheng, G.Y.; Lee, S.W.; Liang, Z.; Lee, H.W.; Yan, K.; Yao, H.; Wang, H.; Li, W.; Chu, S.; Cui, Y. Interconnected hollow carbon nanospheres for stable lithium metal anodes. *Nat. Nanotechnol.* **2014**, *9*, 618–623. [[CrossRef](#)]
135. Yan, K.; Lee, H.-W.; Gao, T.; Zheng, G.; Yao, H.; Wang, H.; Lu, Z.; Zhou, Y.; Liang, Z.; Liu, Z.; et al. Ultrathin Two-Dimensional Atomic Crystals as Stable Interfacial Layer for Improvement of Lithium Metal Anode. *Nano Lett.* **2014**, *14*, 6016–6022. [[CrossRef](#)]
136. Lin, D.; Liu, Y.; Chen, W.; Zhou, G.; Liu, K.; Dunn, B.; Cui, Y. Conformal Lithium Fluoride Protection Layer on Three-Dimensional Lithium by Nonhazardous Gaseous Reagent Freon. *Nano Lett.* **2017**, *17*, 3731–3737. [[CrossRef](#)] [[PubMed](#)]
137. Zhao, J.; Liao, L.; Shi, F.; Lei, T.; Chen, G.; Pei, A.; Sun, J.; Yan, K.; Zhou, G.; Xie, J.; et al. Surface Fluorination of Reactive Battery Anode Materials for Enhanced Stability. *J. Am. Chem. Soc.* **2017**, *139*, 11550–11558. [[CrossRef](#)] [[PubMed](#)]
138. Yan, C.; Cheng, X.-B.; Yao, Y.-X.; Shen, X.; Li, B.-Q.; Li, W.-J.; Zhang, R.; Huang, J.-Q.; Li, H.; Zhang, Q. An Armored Mixed Conductor Interphase on a Dendrite-Free Lithium-Metal Anode. *Adv. Mater.* **2018**, *30*, e1804461. [[CrossRef](#)] [[PubMed](#)]

139. Kozen, A.C.; Lin, C.-F.; Pearse, A.J.; Schroeder, M.A.; Han, X.; Hu, L.; Lee, S.-B.; Rubloff, G.W.; Noked, M. Next-Generation Lithium Metal Anode Engineering via Atomic Layer Deposition. *ACS Nano* **2015**, *9*, 5884–5892. [[CrossRef](#)] [[PubMed](#)]
140. Song, J.; Lee, H.; Choo, M.-J.; Park, J.-K.; Kim, H.-T. Ionomer-Liquid Electrolyte Hybrid Ionic Conductor for High Cycling Stability of Lithium Metal Electrodes. *Sci. Rep.* **2015**, *5*, 14458. [[CrossRef](#)] [[PubMed](#)]
141. Li, N.-W.; Shi, Y.; Yin, Y.-X.; Zeng, X.-X.; Li, J.-Y.; Li, C.-J.; Wan, L.-J.; Wen, R.; Guo, Y.-G. Inside Cover: A Flexible Solid Electrolyte Interphase Layer for Long-Life Lithium Metal Anodes. *Angew. Chem. Int. Ed.* **2018**, *57*, 1422. [[CrossRef](#)]
142. Belov, D.; Yarmolenko, O.; Peng, A.; Efimov, O. Lithium surface protection by polyacetylene in situ polymerization. *Synth. Met.* **2006**, *156*, 745–751. [[CrossRef](#)]
143. Cui, L.F.; Ruffo, R.; Chan, C.K.; Peng, H.; Cui, Y. Crystalline-amorphous core–shell silicon nanowires for high capacity and high current battery electrodes. *Nano Lett.* **2009**, *9*, 491–495. [[CrossRef](#)]
144. Nie, M.; Abraham, D.P.; Chen, Y.; Bose, A.; Lucht, B.L. Silicon Solid Electrolyte Interphase (SEI) of Lithium Ion Battery Characterized by Microscopy and Spectroscopy. *J. Phys. Chem. C* **2013**, *117*, 13403–13412. [[CrossRef](#)]
145. Chan, C.K.; Ruffo, R.; Hong, S.S.; Cui, Y. Surface chemistry and morphology of the solid electrolyte interphase on silicon nanowire lithium-ion battery anodes. *J. Power Sources* **2009**, *189*, 1132–1140. [[CrossRef](#)]
146. Lu, Z.; Liu, N.; Lee, H.-W.; Zhao, J.; Li, W.; Li, Y.; Cui, Y. Nonfilling Carbon Coating of Porous Silicon Micrometer-Sized Particles for High-Performance Lithium Battery Anodes. *ACS Nano* **2015**, *9*, 2540–2547. [[CrossRef](#)] [[PubMed](#)]
147. Liu, N.; Lu, Z.; Zhao, J.; McDowell, M.T.; Lee, H.W.; Zhao, W.; Cui, Y. A pomegranate-inspired nanoscale design for large-volume-change lithium battery anodes. *Nat. Nanotechnol.* **2014**, *9*, 187–192. [[CrossRef](#)]
148. Lee, H.-W.; Muralidharan, P.; Mari, C.M.; Ruffo, R.; Kim, D.K. Facile synthesis and electrochemical performance of ordered $\text{LiNi}_{0.5}\text{Mn}_{1.5}\text{O}_4$ nanorods as a high power positive electrode for rechargeable Li-ion batteries. *J. Power Sources* **2011**, *196*, 10712–10716. [[CrossRef](#)]
149. Padhi, A.K.; Nanjundaswamy, K.S.; Goodenough, J.B. Phospho-olivines as Positive-Electrode Materials for Rechargeable Lithium Batteries. *J. Electrochem. Soc.* **1997**, *144*, 1188. [[CrossRef](#)]
150. Liang, G.; Peterson, V.K.; See, K.W.; Guo, Z.; Pang, W.K. Developing high-voltage spinel $\text{LiNi}_{0.5}\text{Mn}_{1.5}\text{O}_4$ cathodes for high-energy-density lithium-ion batteries: Current achievements and future prospects. *J. Mater. Chem. A* **2020**, *8*, 15373–15398. [[CrossRef](#)]
151. Hai, B.; Shukla, A.K.; Duncan, H.; Chen, G. The effect of particle surface facets on the kinetic properties of $\text{LiNi}_{0.5}\text{Mn}_{1.5}\text{O}_4$ cathode materials. *J. Mater. Chem A* **2013**, *1*, 759–769. [[CrossRef](#)]
152. Ma, J.; Cui, G.; Chen, L. Surface and Interface Issues in Spinel $\text{LiNi}_{0.5}\text{Mn}_{1.5}\text{O}_4$: Insights into a Potential Cathode Material for High Energy Density Lithium Ion Batteries. *Chem. Mater.* **2016**, *28*, 3578–3606. [[CrossRef](#)]
153. Chen, J.; Huang, Z.; Zeng, W.; Cao, F.; Na, J.; Tina, W.; Mu, S. Synthesis, Modification, and Lithium-Storage Properties of Spinel $\text{LiNi}_{0.5}\text{Mn}_{1.5}\text{O}_4$. *ChemElectroChem* **2021**, *8*, 608–624. [[CrossRef](#)]
154. Piao, J.-Y.; Gu, L.; Wei, Z.; Ma, J.; Wu, J.; Yang, W.; Gong, Y.; Sun, Y.-G.; Duan, S.-Y.; Tao, X.-S.; et al. Phase Control on Surface for the Stabilization of High Energy Cathode Materials of Lithium Ion Batteries. *J. Am. Chem. Soc.* **2019**, *141*, 4900–4907. [[CrossRef](#)]
155. Xiao, B.; Liu, H.; Liu, J.; Sun, Q.; Wang, B.; Kaliyappan, K.; Zhao, Y.; Banis, M.N.; Liu, Y.; Xu, L.; et al. Nanoscale Manipulation of Spinel Lithium Nickel Manganese Oxide Surface by Multisite Ti Occupation as High-Performance Cathode. *Adv. Mater.* **2017**, *29*, 1703764. [[CrossRef](#)]
156. Kim, J.W.; Kim, D.H.; Oh, D.Y.; Lee, H.; Kim, J.H.; Lee, J.H.; Jung, Y.S. Surface chemistry of $\text{LiNi}_{0.5}\text{Mn}_{1.5}\text{O}_4$ particles coated by Al_2O_3 using atomic layer deposition for lithium-ion batteries. *J. Power Sources* **2015**, *274*, 1254–1262. [[CrossRef](#)]
157. Zou, Z.; Xu, H.; Zhang, H.; Tang, Y.; Cui, G. Electrolyte Therapy for Improving the Performance of $\text{LiNi}_{0.5}\text{Mn}_{1.5}\text{O}_4$ Cathodes Assembled Lithium-Ion Batteries. *ACS Appl. Mater. Interfaces* **2020**, *12*, 21368–21385. [[CrossRef](#)]
158. Rong, H.; Xu, M.; Xing, L.; Li, W. Enhanced cyclability of $\text{LiNi}_{0.5}\text{Mn}_{1.5}\text{O}_4$ cathode in carbonate based electrolyte with incorporation of tris(trimethylsilyl)phosphate (TMSP). *J. Power Sources* **2014**, *261*, 148–155. [[CrossRef](#)]
159. Kim, S.; Kim, M.; Choi, I.; Kim, J.J. Quercetin as electrolyte additive for $\text{LiNi}_{0.5}\text{Mn}_{1.5}\text{O}_4$ cathode for lithium-ion secondary battery at elevated temperature. *J. Power Sources* **2016**, *336*, 316–324. [[CrossRef](#)]
160. Wang, X.; Xue, W.-D.; Hu, K.; Li, Y.; Li, Y.; Huang, R.-Y. Adiponitrile as Lithium-Ion Battery Electrolyte Additive: A Positive and Peculiar Effect on High-Voltage Systems. *ACS Appl. Energy Mater.* **2018**, *1*, 5347–5354. [[CrossRef](#)]
161. Wu, B.; Ren, Y.; Mu, D.; Liu, X.; Wu, F. Electrochemical performance of 5 V $\text{LiNi}_{0.5}\text{Mn}_{1.5}\text{O}_4$ cathode modified with lithium carbonate addition in electrolyte. *J. Power Sources* **2014**, *272*, 183–189. [[CrossRef](#)]
162. Li, C.; Zhao, Y.; Zhang, H.; Liu, J.; Jing, J.; Cui, X.; Li, S. Compatibility between $\text{LiNi}_{0.5}\text{Mn}_{1.5}\text{O}_4$ and electrolyte based upon lithium bis(oxalate)borate and sulfolane for high voltage lithium-ion batteries. *Electrochim. Acta* **2013**, *104*, 134–139. [[CrossRef](#)]
163. Ren, X.; Chen, S.; Lee, H.; Mei, D.; Engelhard, M.H.; Burton, S.D.; Zhao, W.; Zheng, J.; Li, Q.; Ding, M.S.; et al. Localized High-Concentration Sulfone Electrolytes for High-Efficiency Lithium-Metal Batteries. *Chem* **2018**, *4*, 1877–1892. [[CrossRef](#)]
164. Matsumoto, K.; Martinez, M.; Gutel, T.; Mailley, S.; De Vito, E.; Patoux, S.; Inoue, K.; Utsugi, K. Stability of trimethyl phosphate non-flammable based electrolyte on the high voltage cathode ($\text{LiNi}_{0.5}\text{Mn}_{1.5}\text{O}_4$). *J. Power Sources* **2015**, *273*, 1084–1088. [[CrossRef](#)]
165. Zheng, X.; Liao, Y.; Zhang, Z.; Zhu, J.; Ren, F.; He, H.; Xiang, Y.; Zheng, Y.; Yang, Y. Exploring high-voltage fluorinated carbonate electrolytes for $\text{LiNi}_{0.5}\text{Mn}_{1.5}\text{O}_4$ cathode in Li-ion batteries. *J. Energy Chem.* **2020**, *42*, 62–70. [[CrossRef](#)]

-
166. Cao, X.; He, X.; Wang, J.; Liu, H.; Röser, S.; Rad, B.R.; Evertz, M.; Streipert, B.; Li, J.; Wagner, R.; et al. High Voltage $\text{LiNi}_{0.5}\text{Mn}_{1.5}\text{O}_4/\text{Li}_4\text{Ti}_5\text{O}_{12}$ Lithium Ion Cells at Elevated Temperatures: Carbonate- versus Ionic Liquid-Based Electrolytes. *ACS Appl. Mater. Interfaces* **2016**, *8*, 25971–25978. [[CrossRef](#)] [[PubMed](#)]
167. Dai, W.; Dong, N.; Xia, Y.; Chen, S.; Luo, H.; Liu, Y.; Liu, Z. Localized concentrated high-concentration electrolyte enhanced stability and safety for high voltage Li-ion batteries. *Electrochim. Acta* **2019**, *320*, 134633. [[CrossRef](#)]
168. Noh, H.-J.; Youn, S.; Yoon, C.S.; Sun, Y.-K. Comparison of the structural and electrochemical properties of layered Li $[\text{Ni}_x\text{Co}_y\text{Mn}_z]\text{O}_2$ ($x = 1/3, 0.5, 0.6, 0.7, 0.8$ and 0.85) cathode material for lithium-ion batteries. *J. Power Sources* **2013**, *233*, 121–130. [[CrossRef](#)]
169. Manthiram, A.; Knight, J.C.; Myung, S.-T.; Oh, S.-M.; Sun, Y.-K. Nickel-Rich and Lithium-Rich Layered Oxide Cathodes: Progress and Perspectives. *Adv. Energy Mater.* **2016**, *6*, 1501010. [[CrossRef](#)]
170. Lim, B.-B.; Myung, S.-T.; Yoon, C.S.; Sun, Y.-K. Comparative Study of Ni-Rich Layered Cathodes for Rechargeable Lithium Batteries: $\text{Li}[\text{Ni}_{0.85}\text{Co}_{0.11}\text{Al}_{0.04}]\text{O}_2$ and $\text{Li}[\text{Ni}_{0.84}\text{Co}_{0.06}\text{Mn}_{0.09}\text{Al}_{0.01}]\text{O}_2$ with Two-Step Full Concentration Gradients. *ACS Energy Lett.* **2016**, *1*, 283–289. [[CrossRef](#)]
171. Li, W.; Dolocan, A.; Oh, P.; Celio, H.; Park, S.; Cho, J.; Manthiram, A. Dynamic behaviour of interphases and its implication on high-energy-density cathode materials in lithium-ion batteries. *Nat. Commun.* **2017**, *8*, 14589. [[CrossRef](#)] [[PubMed](#)]